Paramagnetic Resonance and Spin-Lattice Relaxation for Ytterbium in Yttrium Ethyl Sulfate; Large Anisotropies and Evidence for Electric Dipole Transitions*

J. P. Wolfe and C. D. Jeffries
Department of Physics, University of California, Berkeley, California 94720
(Received 1 March 1971)

Paramagnetic resonance is detected for $^{172}Yb^{3+}$ ions diluted in crystals of $Y(C_2H_5SO_4)_3 \cdot 9H_2O$ at temperatures $1.2 \leq T \leq 4.2$ °K, and $\nu = 23$ GHz, for $0 \leq \theta \leq 70°$, where θ is the angle between the crystal c axis and $\vec{H}$. We find $g_{\parallel} = 3.328 \pm 0.005$; $g_{\perp}$ is not directly measured, but estimated to be $g_{\perp} \approx 0.01$ from the resonance intensity at $\theta = 0°$. An observed angular variation of 10^2 in linewidth can be explained by a c-axis wander throughout the crystal, of order $(\delta\theta)_{rms} \approx 0.05°$. A striking angular variation in line intensity, of the form $(\tan^2\theta)/\cos\theta$ over five orders of magnitude, is used to deduce that the observed line is an electric dipole transition rather than the usual magnetic dipole transition, observed only at $\theta = 0°$. This is further confirmed by placement of the crystal in the cavity in regions of maximum electric or magnetic field. The electric dipole transition comes about by the combined action of the Zeeman perturbation and admixtures of even-parity states into the odd-parity $4f^{13}$ configuration by odd terms in the C_{3h} crystal field. The direct spin-lattice relaxation rate is measured by a microwave pulse-recovery method and found to be $T_{1d}^{-1} = 134T \tan^2\theta$ sec^{-1} (T in °K) at constant frequency $\nu = 23.11$ GHz, which corresponds to $T_{1d}^{-1} = 2.4 \times 10^{-17} H^5 \cos^3\theta \sin^2\theta \coth(h\nu/2kT)$ sec^{-1} (H in oersteds), the theoretically expected form. At large angles the data indicate a phonon bottleneck. It was found that the EPR signal could be reduced by optical pumping in the 1- to 3-μ region. An optical pulse-recovery method was used to measure the Raman spin-lattice relaxation rate, $T_{1R}^{-1} = 0.0135T^9$ sec^{-1}. These data are of central importance in the analysis of nuclear spin refrigerators utilizing this unusually anisotropic crystal.

I. INTRODUCTION

In terms of its low-lying energy levels, Yb^{3+} is one of the few simple rare-earth ions. This is because the $4f^{13}$ configuration lacks one electron for a filled shell and may be simply approximated by a single "hole." As in Ce^{3+}, which has a single electron in the $4f$ shell, there are only 14 basis states, which, in the presence of spin-orbit coupling, are split into two multiplets, $^2F_{7/2}$ and $^2F_{5/2}$, the $J = \frac{7}{2}$ multiplet lying lowest in ytterbium. For Yb diluted in $Y(C_2H_5SO_4)_3 \cdot 9H_2O$, abbreviated as YES: Yb, the C_{3h} crystal field splits this multiplet into four Kramers doublets, as shown in Fig. 1. This paper is concerned with paramagnetic resonance and spin relaxation in the $J_z = \pm\frac{3}{2}$ ground doublet.

An important and unique feature of the YES: Yb crystal is that the g factor of the ground doublet is extremely anisotropic. In fact, from Fig. 1, it is clear that to first order the Zeeman interaction $\mathcal{H}_Z = \mu_B g_L \vec{J} \cdot \vec{H}$ does not split the ground doublet when the crystal c axis is perpendicular to $\vec{H}$, since $g_{\perp} = g_L \langle -\frac{3}{2} | J_+ + J_- | +\frac{3}{2} \rangle = 0$; g_L is the Landé g factor. This is due to the circumstance that the C_{3h} crystal field operators V_2^0, V_4^0, V_6^0, and V_6^6 do not mix the $\pm\frac{3}{2}$ doublet to any other state in the $J = \frac{7}{2}$ multiplet. Admixtures from the $J = \frac{5}{2}$ multiplet, which is 10 000 cm^{-1} away, do not contribute to $g_{\perp}$. Actually $\mathcal{H}_Z$ itself admixes the ground doublet with the crystal field excited states in the $J = \frac{7}{2}$ multiplet, giving rise to a third-order Zeeman splitting, but this effect is small in fields below 20 kOe, with the result that $g_{\perp}$ is very small, of order of the proton nuclear g factor. Consequently, YES: Yb has been successfully employed in a proton spin refrigerator scheme[1-3] which relies both on cross relaxation between electrons and protons and on an extremely anisotropic electron relaxation time. A detailed theoretical analysis of the spin refrigerator requires a knowledge of the g factors and the electron spin-lattice relaxation rates. In fact, inadequate prior experimental knowledge of these essential parameters provided the initial motivation for our resonance and relaxation study of this important and peculiar rare-earth ion.

Unfortunately, the small value of $g_{\perp}$ also creates experimental difficulties not present for other ions; namely, the paramagnetic resonance absorption is quite weak. The reason for this is that the J_+ and J_- operators giving rise to magnetic dipole transitions have zero matrix elements between pure $|+\frac{3}{2}\rangle$ and $|-\frac{3}{2}\rangle$ states. However, admixing of excited crystal field states into these zero-order states by the Zeeman Hamiltonian does yield, as we will show, a very small transition probability. In fact, Schmugge[4] first observed a weak microwave paramagnetic resonance (EPR) in LaES: Yb, a crystal very similar to YES: Yb, and it was thought that it was a weak magnetic dipole transition. However,

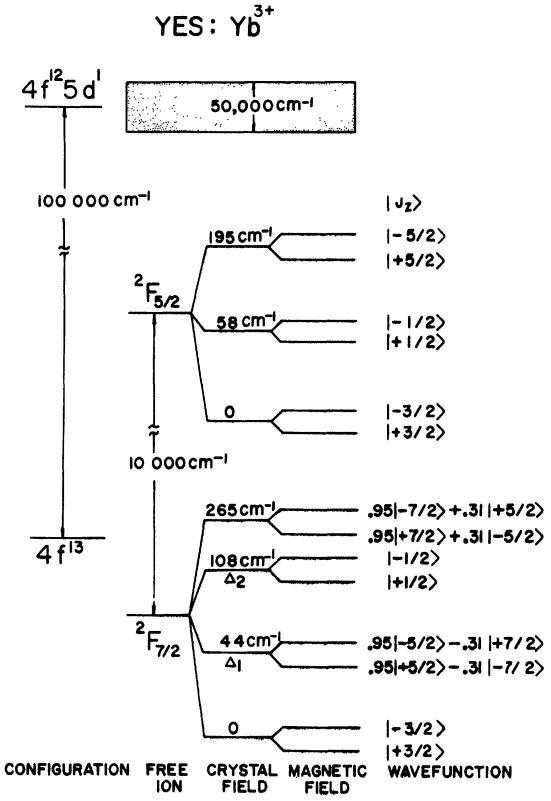

FIG. 1. Energy levels of Yb^{3+} in yttrium ethyl sulfate. For the ground multiplet $J=\frac{7}{2}$, the odd-parity wave functions for $\vec{H} \| c \| z$ are written in terms of the basis states $|J=\frac{7}{2}, J_z\rangle$. This figure is based on Ref. 1, with modifications by Ballard, Ref. 3, using new data in Ref. 9.

one of the principal results of this paper will be to show that the EPR signals observed in YES: Yb (and presumably also in LaES: Yb) are predominately electric dipole transitions induced by the microwave electric field component. This unusual effect comes about because of admixtures by odd crystal field terms of even-parity configurations, e. g., $4f^{12}5d$, into the odd-parity $4f^{13}$ configuration of the ground state.

Other new results are the observation and interpretation of a large angular variation in linewidth, and the observation that the EPR signal may be optically pumped.

II. APPARATUS

A sensitive 1-cm superheterodyne spectrometer is used for both EPR detection and the relaxation time experiments. The noise figure of the receiver was measured to be 12 dB. The cavity and sample were immersed in liquid He^4 in a standard metal Dewar, between the poles of a rotatable electromagnet producing up to 19 kOe in a horizontal direction.

A tunable, high-Q microwave cavity with a rotating crystal mount was employed throughout this experiment. The cavity mode was TE_{011}, and the samples were usually mounted in the center of the cylindrical cavity as shown in Fig. 2. The crystal could be rotated about a horizontal axis, and the magnetic field rotated in a horizontal plane, so that the crystal c axis could be aligned accurately along the magnetic field. This arrangement was essential for measurement of $g_{\|}$. In addition, the cavity was designed so that the sample could be optically pumped, an experiment which will be described later. For measurements of the g factor and the linewidth, a derivative of the absorption line was recorded in the usual way, using field modulation and lock-in detection.

A block diagram of the relaxation time apparatus is shown in Fig. 3, and is similar to earlier versions used in this laboratory.[5] The microwaves were repetitively switched from a high level (saturating the EPR) to a low level, where the recovery of the spins to thermal equilibrium was monitored on an oscilloscope. The signal klystron was a $\frac{1}{2}$-W OKI-type 55V11 klystron, and a 10-dB directional coupler to the receiver was used rather than the usual hybrid-T arrangement. This had the disad-

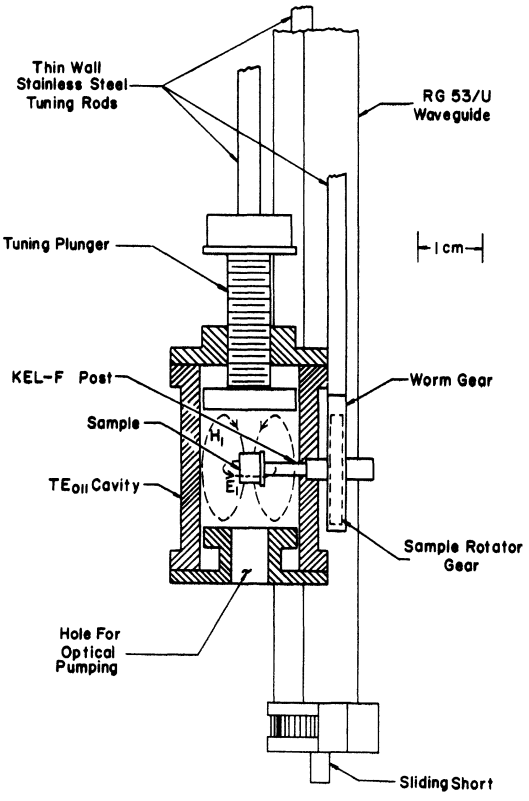

FIG. 2. Microwave cavity, with rotatable sample holder. For clarity, gear mounting is not shown.

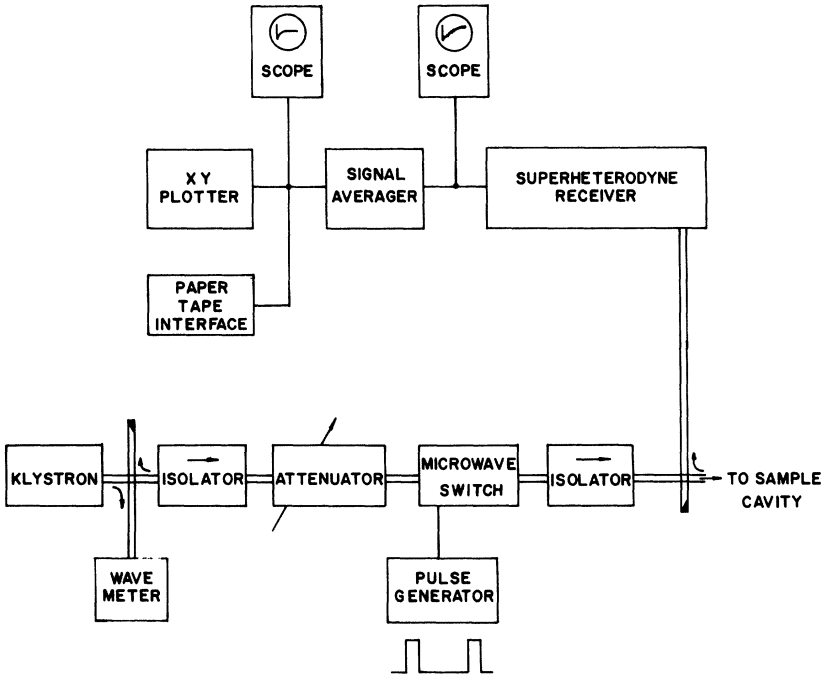

FIG. 3. Block diagram of apparatus for pulse-recovery method of measuring spin-lattice relaxation rates.

vantage of a 10-dB loss of signal, but allowed maximum power into the cavity for saturating the spins; this was necessary in YES: Yb because of the unusually small transition probability. The microwave diode switch, a Philco model No. S-6510, had a 2-dB insertion loss and a 30-dB on-off ratio and was driven with a Tektronix pulse generator. One notable complication of this scheme was that high-power pulses caused heating of the cavity walls and formation of tiny He bubbles, sometimes shifting the cavity resonance frequency. This problem was minimized by using a high on-off ratio of the switch (i.e., low monitor levels) and long intervals between pulses, as well as short pulse lengths where possible. Also, it was found necessary to automatically frequency control the signal klystron directly to the cavity resonance, using frequency modulation at 60 kHz and lock-in detection.

Small signal-to-noise ratios made necessary the use of a signal averaging computer, Nuclear Data model No. ND800 Enhancetron. The averaged signal was recorded on an x-y plotter and later plotted on semilog paper for determination of the recovery time. In most instances, the recovery signal, which was stored digitally in the signal averager, was then punched onto paper tape and later fed into an IBM 1620 computer for curve fitting to a single exponential.

Crystals. The results reported here were obtained using YES: Yb crystals grown by McColl for his spin refrigerator experiments.[2] The crystals were grown with 97.1% isotopically enriched YB^{172} ($I=0$). The $Y_2(SO_4)_3 \cdot 8H_2O$ used for making the YES crystal was 99.999% pure in yttrium. Two of the crystals used were grown in pure D_2O and are designated as 1% and 2% YES($9D_2O$): Yb, where the shorthand notation is used for $[Y(C_2H_5SO_4)_3 \cdot 9D_2O]$. No attempt was made to deuterate the ethyl radicals. McColl estimates that 80% of the H_2O is replaced by D_2O in these crystals.

III. ELECTRON PARAMAGNETIC RESONANCE OF YTTERBIUM

A. g Factors

The Yb^{3+} EPR was observed from $\theta = 0°$ to $\theta = 74°$ at 23 GHz and $T = 1.5\,°K$, where θ is the angle between the external magnetic field and the crystal c axis. For angles above $\theta = 10°$, a single resonance line was observed (since $I = 0$ for all the crystals considered); however, near the c axis the EPR spectrum exhibited a small amount of structure, displayed in Fig. 4(a). The structure at $\theta = 0°$ is the subject of some conjecture, in particular, the two resolved satellite lines. The deuterated sample exhibited a sharper and stronger main line with relatively less intense satellites, as shown in Fig. 5; the lines are sharper because of the reduced contribution from the deuteron nuclear moments. The splitting of about 15 Oe between the main line and each satellite is not far from the 12.3 Oe we calculate for the next-nearest-neighbor pair lines, due to pure magnetic dipolar interaction between two neighboring Yb^{3+} ions. In fact, the intensity ratio of 2.4 between the two satellites is exactly what one expects for 40% polarized electrons at

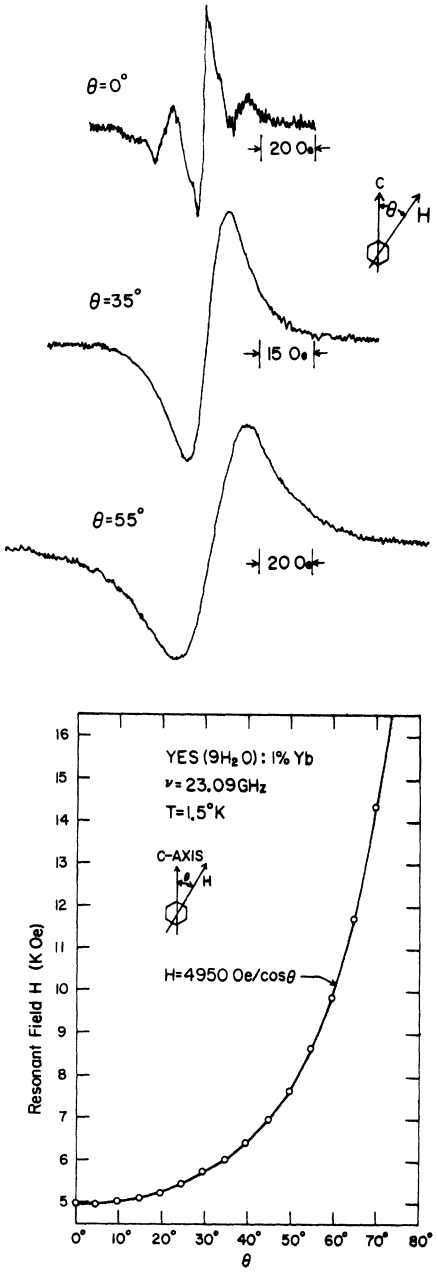

FIG. 4. (a) Derivative of EPR resonance in $YES(9H_2O)$: 1% Yb at 1.5 °K, $\nu = 23.09$ GHz. Note structure at $\theta = 0°$, and increasing width and loss of structure at larger θ. (b) Circles are the measured resonance field vs θ for the crystal of (a). The solid curve is Eq. (1); the good fit shows $g_\perp \approx 0$, and determines $g_\parallel$, Eq. (2a).

the measured 1.41 °K. The intensity of these pair lines is most likely enhanced by the reduced site symmetry for adjacent Yb ions resulting in an increased $g_\perp$. The C_{3h} symmetry is not lowered for nearest-neighbor ions, however, and the corresponding pair lines were not detected. Additional weak resonances, attributable to Yb ions in differing sites,[6] were also found.

The measured central-line resonant field versus angle is shown in Fig. 4(b). The resonance condition is

$$h\nu = (g_\parallel^2 \cos^2\theta + g_\perp^2 \sin^2\theta)^{1/2} \mu_B H \ ;$$

$$H = H_\parallel / \cos\theta \quad \text{with} \quad H_\parallel \equiv h\nu / g_\parallel \mu_B \ , \qquad (1)$$

which is represented as the solid curve in Fig. 4(b), with $H_\parallel = 4950$ Oe. The c axis was found by successively adjusting the crystal orientation about a horizontal axis and the magnetic field in the horizontal plane until the resonant field was minimized. Field measurements were made with a rotating-coil gaussmeter, and the Yb g factor was obtained by comparison with a standard g marker also in the cavity. Our results for two crystals are

$$g_\parallel = 3.328 \pm 0.005 \text{ for } YES(9H_2O): 1\% \text{ Yb} \ , \qquad (2a)$$

$$g_\parallel = 3.335 \pm 0.002 \text{ for } YES(9D_2O): 2\% \text{ Yb} \ . \qquad (2b)$$

Cooke *et al.*[7] measure $g_\parallel = 3.40 \pm 0.07$ in YbES by magnetic susceptibility, and Schmugge[4] found $g_\parallel = 3.35 \pm 0.07$ in a dilute LaES: Yb crystal. Our result is consistent with, but more precise than, these early results, on similar but not identical crystals.

Our measured values, Eqs. (2), are about 3% lower than the value predicted for pure $|J = \frac{7}{2}, J_z = \pm\frac{3}{2}\rangle$ states,

$$g_\parallel = 2g_L \langle +\tfrac{3}{2} | J_z | +\tfrac{3}{2} \rangle = 3g_L = 3.429 \ , \qquad (3)$$

where $g_L = \frac{8}{7}$ is the Landé g factor for the $J = \frac{7}{2}$ multi-

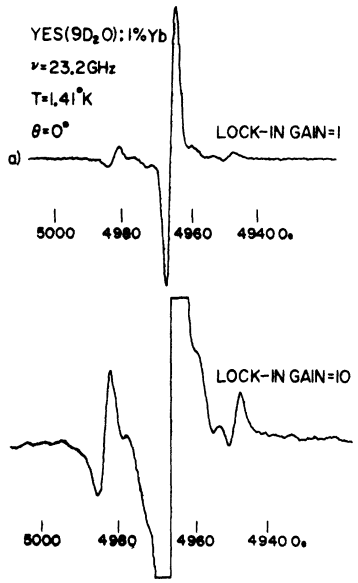

FIG. 5. Derivative of EPR resonance in $YES(9D_2O)$: 1% Yb at $\theta = 0$, showing structure, possibly due to Yb-Yb dipolar interaction.

plet. One possible source for this discrepancy is admixtures of $J=\frac{5}{2}$ states. The C_{3h} crystal field terms available are V_2^0, V_4^0, V_6^0, and V_6^6. The V_6^6 term has no effect on a $\pm\frac{1}{2}$ doublet, but the $V_{2,4,6}^0$ terms will connect the ground state with the $\pm\frac{1}{2}$ states in the $J=\frac{5}{2}$ multiplet. This so-called J mixing is calculated in Appendix A; the necessary ground states to yield $g_\parallel = 3.33$ are

$$|+\tfrac{3}{2}\rangle^1 = 0.9985\ |\tfrac{7}{2},+\tfrac{3}{2}\rangle + 0.055\ |\tfrac{5}{2},+\tfrac{3}{2}\rangle\ , \qquad (4a)$$

$$|-\tfrac{3}{2}\rangle^1 = 0.9985\ |\tfrac{7}{2},-\tfrac{3}{2}\rangle - 0.055\ |\tfrac{5}{2},-\tfrac{3}{2}\rangle\ , \qquad (4b)$$

where the notation $|J, J_z\rangle$ is employed.

There is now the question of whether the spectroscopically measured values of $V_{2,4,6}^0$ can produce the needed mixing. Using the appropriate terms in the crystal field Hamiltonian,[8]

$$\mathcal{H}_c = A_2^0\langle r^2\rangle \alpha O_2^0 + A_4^0\langle r^4\rangle \beta O_4^0 + A_6^0\langle r^6\rangle \gamma O_6^0\ , \qquad (5)$$

and Wheeler's[9] values for the parameters $A_2^0\langle r^2\rangle = 155.4\ \text{cm}^{-1}$, $A_4\langle r^4\rangle = -57.7\ \text{cm}^{-1}$, $A_6^0\langle r^6\rangle = -25.6\ \text{cm}^{-1}$ from far-infrared spectroscopy, we find

$$\frac{\langle \frac{5}{2},\frac{3}{2}|\mathcal{H}_c|\frac{7}{2},\frac{3}{2}\rangle}{\delta} = -\frac{17\ \text{cm}^{-1}}{10^4\ \text{cm}^{-1}} = -0.0017\ , \qquad (6)$$

where the matrix elements of $O_{2,4,6}^0$ between J multiplets are given by Elliot and Stevens,[8] and the splitting $\delta = 10\,000\ \text{cm}^{-1}$ between the $J=\frac{5}{2}$ and $J=\frac{7}{2}$ multiplets has also been used.[9] Since the magnitude of Eq. (6) is much less than the required value 0.055, Eq. (A1), this indicates that the J mixing is not sufficient to explain the measured $g_\parallel$.

Apart from J mixing, we may also consider the possibility that there is a departure from reflection symmetry, lowering the symmetry to C_{3v} and introducing V_4^3 and V_6^3 terms into the crystal potential. However, these operators will not connect the $J_z=\pm\frac{3}{2}$ states to any other excited states within the $J=\frac{7}{2}$ multiplet. Further lowering of the crystal symmetry to C_2 would result in a $g_\parallel$ shift, but the needed $V_4^4 \sim 5\ \text{cm}^{-1}$ is inconsistent with the small measured $g_\perp$.

A final possibility considered here is that the dynamic crystal field terms, arising from lattice vibrations, cause the required mixing among the $J=\frac{7}{2}$ states. For the case of Ce^{3+} in YES, this has indeed been shown[10,11] to be the cause of an 8% lower experimental value of $g_\parallel$ than that calculated from the static crystal field terms. For YES: Yb our $g_\parallel$ value is 3% lower, and the reduction is quite possibly due to this same mechanism.

Although we have attempted to determine directly the important parameter $g_\perp$ for YES: Yb by direct resonance experiments using an NMR spectrometer at 20, 80, 160, and 400 MHz, we have been unable to detect a well-defined resonance. At present we can only say that from line-intensity measurements (Sec. III C) our best value is $g_\perp \approx 0.01$, which is considerably larger than the value calculated from third-order Zeeman splitting,[1] $(g_\perp)_3 \approx 3\times10^{-12}\,H^2$, which yields 7.5×10^{-5} at our field of 5 kG.

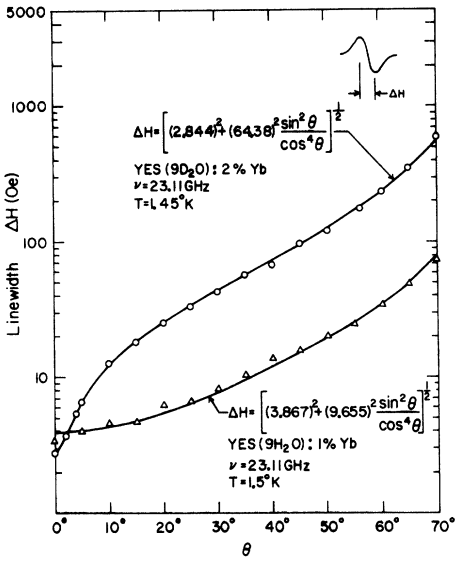

FIG. 6. Peak-to-peak derivative linewidth ΔH vs θ for two YES: Yb crystals. The solid lines are the theoretical expression, Eq. (8).

B. Linewidth

It is found experimentally that the linewidth increases rapidly as θ is increased, as shown in Fig. 6. The data are well explained by considering a Gaussian distribution of c axes throughout the crystal:

$$F(\theta) = (2\pi\langle\Phi^2\rangle_{av})^{-1/2}\exp(-\Phi^2/2\langle\Phi^2\rangle_{av})\ , \qquad (7)$$

where Φ is the angular deviation of a tiny crystallite's c axis from the mean c axis, and $\langle\Phi^2\rangle_{av}^{1/2} \equiv \Phi_{rms}$ is the rms angular deviation for the entire crystal.

It is shown in Appendix B that this leads to a peak-to-peak derivative EPR linewidth given by

$$\Delta H = \left((\Delta H_n)^2 + 4\langle\Phi^2\rangle_{av} H_\parallel^2 \frac{\sin^2\theta}{\cos^4\theta}\right)^{1/2}\ , \qquad (8)$$

where ΔH_n is the contribution to the derivative linewidth due to the local fields of the surrounding nuclei, and θ is the field angle with respect to the mean c axis.

A two-parameter least-squares fit of this function to the data for two crystals is shown as the solid line in Fig. 6. Using $H_\parallel = 4950$ Oe, this fit corresponds to

$$\Delta H_n = 3.87\ \text{Oe} \quad \text{and} \quad \Phi_{rms} = 0.057^\circ \qquad (9a)$$

for the YES($9H_2O$): 1% Yb crystal, and

$$\Delta H_n = 2.84 \text{ Oe} \quad \text{and} \quad \Phi_{rms} = 0.380^\circ \tag{9b}$$

for the YES($9D_2O$): 2% Yb crystal. The deuterated 1% crystal yielded results similar to the deuterated 2% crystal. Thus, for YES: Yb, a very small angular distribution of the c axis explains rather well the large observed anisotropy in the linewidth. Similar effects have been reported and explained by Scott, Stapleton, and Wainstein[12] for three rare-earth ions in LaMN where $g_\parallel$ and $g_\perp$ are quite dissimilar. In fact, their treatment is similar to that given in Appendix B, with the further generalization that there is a distribution in the values of $g_\parallel$ and $g_\perp$, described by the mean-squared deviations $\langle(\delta g_\parallel)^2\rangle_{av}$ and $\langle(\delta g_\perp)^2\rangle_{av}$. For YES: Yb, where $g_\perp \approx 0$, this adds a term $4H_\parallel^2\langle(\delta g_\parallel)^2\rangle_{av}/g_\parallel^2 \cos^2\theta$ inside the square root in Eq. (8). With this additional term we tried a three-parameter fit to the data for both crystals, with the result $\langle(\delta g_\parallel)^2\rangle_{av} \approx 0$, and the values ΔH_n and Φ_{rms} given by Eqs. (9a) and (9b), as before. This result is not unreasonable, since $\Delta H_n = 3.87$ Oe is close to the value 2.85 Oe we calculate due to the dipolar fields at $\theta = 0^\circ$ of the 36 nearest protons around the Yb^{3+} site. Thus the linewidth at $\theta = 0^\circ$ is primarily due to the local proton fields.

We note that for the deuterated crystal ΔH_n is only 27% smaller than for the hydrated crystal, whereas we would expect $\Delta H_n \propto \mu_n[(I+1)/I]^{1/2}$, resulting in a reduction by a factor 3.98. We attribute this discrepancy to the fact that the waters are only about 80% deuterated, and the ethyl groups not at all deuterated; furthermore, the Yb-Yb dipolar interaction is not negligible in this 2% crystal, and contributes about $(1.6)^2$ Oe^2 to the mean-squared linewidth. We further note that Φ_{rms} is 6.5 times larger for the deuterated crystal than the hydrated crystal, leading to a much larger linewidth at $\theta > 5^\circ$. This is not unreasonable, since the partially deuterated crystal is not really a periodic lattice and has considerable local strains and c-axis wander.

C. Intensity

It can be readily seen that for pure $\pm\frac{3}{2}$ states, there would be no observable EPR line, since the J_+ and J_- operators of the rf interaction do not connect these states. In a first attempt to explain the finite EPR intensity and its large angular dependence, we introduce mixing of excited states within the $J = \frac{7}{2}$ manifold into the ground doublet by the static Zeeman interaction,

$$\mathcal{H}_Z = g_L\mu_B H[J_z\cos\theta + \tfrac{1}{2}\sin\theta\,(J_+e^{-i\varphi} + J_-e^{i\varphi})]$$

$$\rightarrow \tfrac{1}{2}g_L\mu_B H\sin\theta(J_+ + J_-)\,, \tag{10}$$

where θ is the angle between the external field and the crystal c axis, and we take $\varphi = 0$ without loss of generality because of axial symmetry. The phase factors must be retained, however, when the symmetry is lowered. The J_z term is omitted because it does not couple $|\pm\frac{3}{2}\rangle$ to an excited state.

In the presence of this interaction the ground doublet becomes

$$|+\tfrac{3}{2}\rangle' = |+\tfrac{3}{2}\rangle + C_2|+\tfrac{1}{2}\rangle + C_1|+\tfrac{5}{2}\rangle\,, \tag{11a}$$

$$|-\tfrac{3}{2}\rangle' = |-\tfrac{3}{2}\rangle + C_2|-\tfrac{1}{2}\rangle + C_1|-\tfrac{5}{2}\rangle\,, \tag{11b}$$

with

$$C_2 = \frac{\sqrt{15}}{2}\frac{g_L\mu_B H\sin\theta}{\Delta_2} = \frac{\sqrt{15}}{2}\frac{g_L\mu_B H_\parallel\tan\theta}{\Delta_2}\,, \tag{12a}$$

$$C_1 = \frac{\sqrt{12}}{2}\frac{g_L\mu_B H_\parallel\tan\theta}{\Delta_1}\,, \tag{12b}$$

where we have used $J_\pm|\pm\frac{1}{2}\rangle = \sqrt{15}\,|\pm\frac{3}{2}\rangle$, $J_\pm|\pm\frac{5}{2}\rangle = \sqrt{12}\,|\pm\frac{3}{2}\rangle$, and to simplify the algebra, we assume a pure $|\pm\frac{5}{2}\rangle$ state at 44 cm^{-1} and a pure $|\mp\frac{7}{2}\rangle$ state at 265 cm^{-1} (cf. Fig. 1).

1. *Magnetic Dipole Transitions*

Now consider the effect of an oscillating rf magnetic field $H_\perp$ perpendicular to both the c axis and the external field. The perturbation is

$$\mathcal{H}_1^M(t) = \tfrac{1}{2}g_L\mu_B H_1(J_+ + J_-)\cos\omega t = \mathcal{H}_1^M\cos\omega t\,. \tag{13}$$

The transition rate resulting from this time-dependent perturbation for a spin system with resonance line-shape function $g(\nu)$, so normalized that $\int_0^\infty g(\nu)\times d\nu = 1$, is given by the expression

$$w_{rf}^M(\nu) = \frac{g(\nu)}{4\hbar^2}\,|'\langle\tfrac{3}{2}|\,\mathcal{H}_1^M\,|-\tfrac{3}{2}\rangle'|^2\,, \tag{14}$$

$$= \frac{g(\nu)}{4\hbar^2}\,|C_2^2\times\tfrac{1}{2}g_L\mu_B H_1\langle\tfrac{1}{2}|\,J_+\,|-\tfrac{1}{2}\rangle|^2\,, \tag{15}$$

$$= \frac{g(\nu)}{4\hbar^2}\,\frac{225}{4}\,\frac{g_L^6\mu_B{}^6H_1{}^2H_\parallel{}^4\tan^4\theta}{\Delta_2^4}\,. \tag{16}$$

For comparison, we write the transition probability for an ordinary system of effective spin $S = \frac{1}{2}$ and effective perpendicular g factor $g_\perp$,

$$w_{rf}^M(\nu) = [g(\nu)/16\hbar^2]\,(g_\perp\mu_B H_1)^2. \tag{17}$$

By comparison to Eq. (16) we see that this equation may be applied to YES: Yb if we take an effective g factor

$$g_\perp^H \equiv g_L\,'\langle\tfrac{3}{2}|\,J_+ + J_-\,|-\tfrac{3}{2}\rangle' = 4g_L C_2^2 \approx 10^{-4}\tan^2\theta\,, \tag{18}$$

where we have evaluated $C_2 = 0.45\times10^{-2}\tan\theta$ from Eq. (12a) using $\Delta_2 = 108$ cm^{-1} and $H_\parallel = 5$ kOe. In other words, this calculation predicts that the transition probability for YES: Yb will be weaker than a normal allowed $g_\perp = 2$ transition by the factor $[(g_\perp)_{Yb}/2]^2 \approx 0.25\times10^{-8}\tan^4\theta$, which would make the

Yb resonance unobservably weak. Furthermore, the prediction that the intensity vanish at $\theta = 0$ is true to any order of static perturbation theory, since the Zeeman perturbation, Eq. (10), vanishes at $\theta = 0$. Contrary to these predictions, the Yb resonance is quite observable at all angles in our apparatus, including $\theta = 0$, when the sample is in the center of the cavity.

To be more quantitative, we have made an experimental estimate of the effective $g_\perp$ from the observed YES: Yb intensity relative to that of a standard g-marker sample. In our apparatus, as is the usual custom, we observe the derivative of the absorption line by field modulation and field sweep; therefore, as shown in Appendix C, for constant microwave frequency $\nu = g(\theta)\mu_B H/h$, it is convenient to define an EPR line "intensity," Eq. (C4),

$$I_\theta = (\Delta H)^2 S = K g_\perp^2 N/g(\theta)\,, \tag{19}$$

where ΔH is the observed peak-to-peak derivative width at angle θ, S is the peak-to-peak signal height at θ, N is the number of spins in sample, and K depends on a number of constant parameters. In order to make an experimental estimate of the effective $g_\perp$ at $\theta = 0$, denoted by $g_\perp^0$, we compared $(\Delta H)^2 S$ observed for YES: Yb with the same quantity for a standard "g-marker" sample of phosphorus-doped silicon,[13] for which $g_\parallel = g_\perp = 2$ and $N_{Si} \cong 10^{14}$ effective spins at the temperature used, $T = 1.5\,^\circ$K, and $\nu = 23$ GHz. Using Eq. (19) and

$$\frac{S(\Delta H)^2|_{Si}}{S(\Delta H)^2|_{Yb}} = \frac{(g_\perp^2)_{Si} N_{Si} (g_\parallel)_{Yb}}{(g_\perp^0)^2 N_{Yb} (g_\parallel)_{Si}}\,, \tag{20}$$

we obtained the following results for $\theta = 0^\circ$:

$$g_\perp^0 = 0.023 \quad \text{for YES}(9D_2O): 1\%\ \text{Yb}\,, \tag{21a}$$

$$g_\perp^0 = 0.012 \quad \text{for YES}(9H_2O): 1\%\ \text{Yb}\,. \tag{21b}$$

In obtaining these results, we used for N_{Yb} the value calculated for the 1% Yb crystals reduced by the rejection ratio 3.3, measured by McColl and Jeffries[2] from optical-absorption measurements; thus, we assumed an actual concentration of 0.3% of Yb in YES. We also assumed similar line shapes for the Yb^{3+} and g-marker resonances; both appeared to be approximately Gaussian. Taking into account the above uncertainties as well as other possible errors, we feel the experimental values of Eqs. (21) are correct within a factor 2.

A likely source of the relatively large value of $g_\perp^0$ at $\theta = 0^\circ$ is random crystal strains of low symmetry. In particular, the static crystal field terms V^2 and V^4 present under C_2 symmetry would mix $|\frac{7}{2}, \mp\frac{1}{2}\rangle$ and $|\frac{7}{2}, \mp\frac{5}{2}\rangle$ states into the $|\frac{7}{2}, \pm\frac{3}{2}\rangle$ ground doublet, resulting in a finite $g_\perp^0$, independent of field magnitude or direction. We find that a magnitude of only 10^{-1} cm^{-1} of V^2 and V^4 terms is needed to explain the above-measured values of $g_\perp^0$.

Therefore, our preliminary conclusion was that the intensity at $\theta = 0^\circ$ may be due to a magnetic dipole transition ($H_1 \perp c$) between low-symmetry crystal field mixed states, but that the angular-dependent magnetic dipole transition rate resulting from Zeeman admixtures into the ground doublet is far too small to account for the relatively large observed intensities away from $\theta = 0^\circ$. Thus we seek other transition mechanisms.

2. *Electric Dipole Transitions*

It is well known that the crystal-field-split states of the $4f^n$ configuration contain admixtures of states of opposite parity, for example, from the $4f^{n-1}5d$ configuration. This idea was originally proposed by Van Vleck[14] in 1936 to explain the nonzero intensities of f-to-f optical transitions, and has been verified by numerous experimenters[15] by observation of electric dipole transitions among states of the $4f$ configuration. Theoretical treatments of this parity mixing problem have been carried out by Judd[16] and Freeman and Watson.[17] In the case of concentrated YbES, Wong[18] observed only electric dipole transitions from the $J = \frac{7}{2}$ ground multiplet to the $J = \frac{5}{2}$ excited multiplet; and Wheeler *et al.*[9] observed only electric dipole transitions in the far infrared among the $J = \frac{7}{2}$ Stark levels.

The admixture of opposite-parity states arises from odd-parity terms in the static crystal field interaction. In the case of a C_{3h} symmetry, the odd-parity terms present are V_3^3 and V_5^3.[19] The admixture of even-parity states into the odd-parity $4f^{13}$ states is a sum over all possible even configurations and a sum over all states with the quantum number M_J within a configuration. For example,

$$|\tfrac{3}{2}\rangle'' = |4f^{13}, \tfrac{7}{2}, \tfrac{3}{2}\rangle + \sum_{\alpha, i} \frac{\langle 4f^{13}, \frac{7}{2}, \frac{3}{2}|V_3^3 + V_5^3|\alpha, i, -\frac{3}{2}\rangle}{E_{\alpha i}} |\alpha, i, -\tfrac{3}{2}\rangle\,, \tag{22}$$

where α is the configuration, and i, M_J label a state within a configuration. The configurations to be summed over include excited configurations such as $4f^{12}5d$ and the so-called broken-shell configurations such as $3d^5 4f^{14}$. Judd[16] has attempted to evaluate similar formidable sums for several rare-earth ions, and, using a number of simplifying assumptions, he has succeeded in explaining the relative intensities of many f-to-f transitions. We have not attempted a theoretical analysis of the states involved or their admixture coefficients, although this may be a tractable problem for the $4f^{13}$ ground configuration; for our purpose we resort to a simpler procedure.

We can illustrate the process and the selection rules involved in our EPR transitions, by replacing the sums of states with a single even-parity $J=\frac{7}{2}$ state. The coefficient of this state will be estimated empirically from the infrared absorption results. The simplified states of the ground multiplet for $\theta=0$ are

$$
\begin{aligned}
|H\rangle &= a\left|\tfrac{7}{2}\right\rangle + b\left|-\tfrac{5}{2}\right\rangle + \epsilon_3\left|+\tfrac{1}{2}\right\rangle_e ,\\
|G\rangle &= a\left|-\tfrac{7}{2}\right\rangle + b\left|\tfrac{5}{2}\right\rangle + \epsilon_3\left|-\tfrac{1}{2}\right\rangle_e ,\\
|F\rangle &= \left|\tfrac{1}{2}\right\rangle + \epsilon_2\left|-\tfrac{5}{2}\right\rangle_e + \epsilon_4\left|+\tfrac{7}{2}\right\rangle_e ,\\
|E\rangle &= \left|-\tfrac{1}{2}\right\rangle + \epsilon_2\left|+\tfrac{5}{2}\right\rangle_e + \epsilon_4\left|-\tfrac{7}{2}\right\rangle_e , \qquad (23)\\
|D\rangle &= a\left|\tfrac{5}{2}\right\rangle - b\left|-\tfrac{7}{2}\right\rangle + \epsilon_1\left|-\tfrac{1}{2}\right\rangle_e ,\\
|C\rangle &= a\left|-\tfrac{5}{2}\right\rangle - b\left|+\tfrac{7}{2}\right\rangle + \epsilon_1\left|+\tfrac{1}{2}\right\rangle_e ,\\
|B\rangle &= \left|\tfrac{3}{2}\right\rangle + \epsilon_0\left|-\tfrac{3}{2}\right\rangle_e ,\\
|A\rangle &= \left|-\tfrac{3}{2}\right\rangle + \epsilon_0\left|+\tfrac{3}{2}\right\rangle_e ,
\end{aligned}
$$

where $a=0.95$, $b=0.31$, $|M\rangle = |4f^{13}, \frac{7}{2}, M\rangle$, and $|M\rangle_e = |\alpha, \frac{7}{2}, M\rangle$ with α labeling an even-parity excited configuration.

The interaction of the ion with an external electric field may be expressed as $\mathcal{H}^E = -\vec{P}\cdot\vec{E} = -P_x E_x$ for a field applied in the crystal x direction, where $\vec{P}$ is the electric dipole operator of the ions. Using the method of operation equivalents, based on the Wigner-Eckart theorem, we replace the first-rank tensor $\vec{P}$ with the angular momentum operator $\vec{J}$ times a reduced matrix element γ. Consequently, for the purpose of calculating matrix elements within the $J=\frac{7}{2}$ ground multiplet we use the operator $\mathcal{H}^E = \gamma E_x J_x$. Therefore, for an oscillating electric field E_1 in the crystal x direction, we have

$$\mathcal{H}_1^E = \tfrac{1}{2}\gamma E_1 (J_+ + J_-)\cos\omega t , \qquad (24)$$

which is understood to connect only states of opposite parity.

This operator will not connect the states $|A\rangle$ and $|B\rangle$, Eqs. (23). Nor will an oscillating electric field along the crystal axis ($E_\parallel$) connect $|A\rangle$ and $|B\rangle$, since $\langle A|\gamma E_\parallel J_z|B\rangle = 3\gamma E_\parallel(\epsilon_0 - \epsilon_0) = 0$. This important cancellation is a consequence of Kramers's theorem.

If we now apply a magnetic field at an angle θ with respect to the c axis, the ground doublet becomes in first order

$$|B\rangle' = |B\rangle + C_2|F\rangle + aC_1|D\rangle + bC_3|G\rangle , \qquad (25a)$$

$$|A\rangle' = |A\rangle + C_2|E\rangle + aC_1|C\rangle + bC_3|H\rangle . \qquad (25b)$$

The electric field induced transition rate between these states is given by

$$w_{rf}^E = \frac{g(\nu)}{4\hbar^2}\left|{}'\langle A\left|\tfrac{1}{2}\gamma E_1(J_+ + J_-)\right|B\rangle'\right|^2$$

$$= \frac{g(\nu)}{16\hbar^2}\left|g_1^E \mu_B E_1\right|^2 , \qquad (26)$$

where

$$g_1^E \equiv (\gamma/\mu_B)\,{}'\langle A\left|(J_+ + J_-)\right|B\rangle' \qquad (27)$$

$$= (2\gamma/\mu_B)\left[C_1(\sqrt{15}\,a\epsilon_1 + \sqrt{12}\,a^2\epsilon_0) + C_2(\sqrt{15}\,\epsilon_0 + \sqrt{12}\,\epsilon_2)\right.$$

$$\left. + C_3(\sqrt{15}\,b\epsilon_3 + \sqrt{12}\,b^2\epsilon_0)\right] . \qquad (28)$$

We notice that for the electric dipole transitions, the matrix elements are linear in the static Zeeman mixing parameters, C_1, C_2, and C_3.

By an argument paralleling that of Appendix C, we can say that for this electric dipole mechanism we expect a derivative line intensity

$$I_\theta^E = K(g_1^E)^2 N/g(\theta) \propto \tan^2\theta/\cos\theta , \qquad (29)$$

as can be seen from Eqs. (12) and (28). Figure 7 shows the observed intensity I_θ for a small (15 mg) YES: Yb crystal located carefully in the cavity in a position of maximum E_1 and minimum H_1, with the crystal c axis perpendicular to E_1. The solid line is $\tan^2\theta/\cos\theta$, showing that for nearly five decades the data are in excellent agreement with Eq. (29). The signal becomes undetectably small for $\theta < 1°$.

We may now estimate empirically a lower limit for the magnitude of I_θ^E, i.e., of the effective g_1^E factor. The far-infrared electric dipole transitions among levels of the $J=\frac{7}{2}$ multiplet are known to be at least an order of magnitude larger than the allowed magnetic dipole transitions, which have not been observed[9]; that is, $|\langle A|\mathcal{H}_1^E|D\rangle|^2 > 10\,|\langle A|\mathcal{H}_1^M|C\rangle|^2$, etc., for equal electric and magnetic field strengths. Taking only the C_1 term in Eq. (28), this implies approximately $\gamma(\sqrt{15}\,\epsilon_1 + \sqrt{12}\,a\epsilon_0) \geq 2\sqrt{30}\,g_L\mu_B a$, from Eqs. (13) and (24), and thus

$$g_1^E \geq 4\sqrt{30}\,C_1 a^2 g_L \approx 0.25\tan\theta , \qquad (30)$$

from Eq. (28) and $C_1 = 1.1\times10^{-2}\tan\theta$ from Eq. (12b). As we will show, this predicted value of g_1^E is approximately verified.

To summarize, we assume that the total EPR transition probability is the sum of Eqs. (17) and (26):

$$w_{rf} = \frac{g(\nu)}{16\hbar^2}(g_1^0\mu_B H_1)^2 + \frac{g(\nu)}{16\hbar^2}(g_1^E\mu_B E_1)^2 , \qquad (31)$$

where we have chosen the incoherent sum of magnetic and electric transition rates because of the random nature of the crystal strains producing the

magnetic dipole contribution. The data seem to favor this choice over a coherent sum of rates, which would predict a θ dependence, $w_{rt} \propto (A + B \times \tan\theta)^2$, and also a considerable φ dependence.

For a given sample location in the microwave cavity, where average $E_1^\perp$ over the sample is denoted $\overline{E}_\perp$ and the average $H_1^\perp$ over the sample is denoted $\overline{H}_\perp$, and $g_\perp^E = G\tan\theta$, the total EPR intensity is

$$I_\theta = \frac{KN}{g(\theta)}\left[(g_\perp^0)^2 + \left(\frac{\overline{E}_\perp}{\overline{H}_\perp}\right)^2 G^2\tan^2\theta\right] \quad . \tag{32}$$

A series of three experiments was conducted to confirm this prediction. A YES($9D_2O$) : 2% Yb sample was oriented in a position of (a) maximum $H_\perp$, (b) maximum $E_\parallel$, and (c) maximum $E_\perp$. The results of these experiments, shown in Fig. 8, were that the transition at $\theta = 0°$ is completely magnetic dipole with $H_1^\perp$ polarization, and the transition away from $\theta = 0°$ is predominantly electric dipole with $E_1^\perp$ polarization. The angular variation of the intensity in all three cases was due to nonzero $\overline{E}_\perp$ over the finite sample volume. The relative intensity for these three experiments was determined by comparison with a g marker glued to the bottom of the cavity. In addition, the ratio of the Yb^{3+} signal at $\theta = 0°$ to the signal of small traces of Nd^{3+} within the sample was the same for all three experiments, attesting to the complete cancellation of large terms in the aforementioned $J_z E_\parallel$ matrix element.

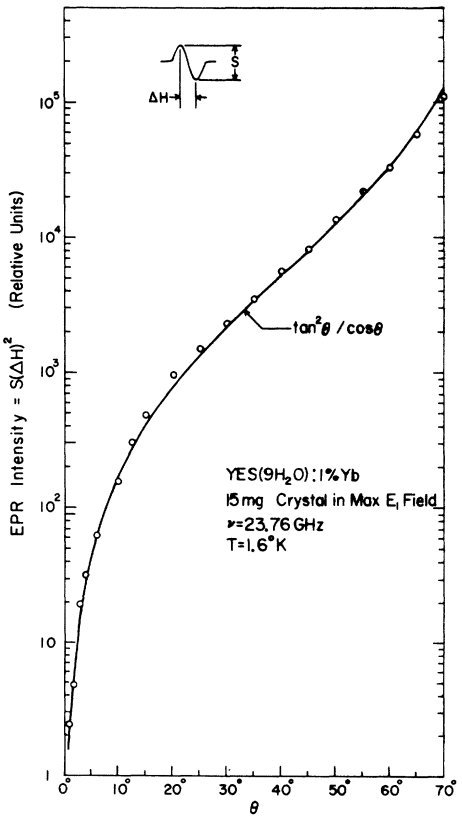

FIG. 7. Angular variation of the EPR intensity I_θ, defined by Eq. (19). The solid line is the theoretical dependence, Eq. (29), for electric dipole transitions.

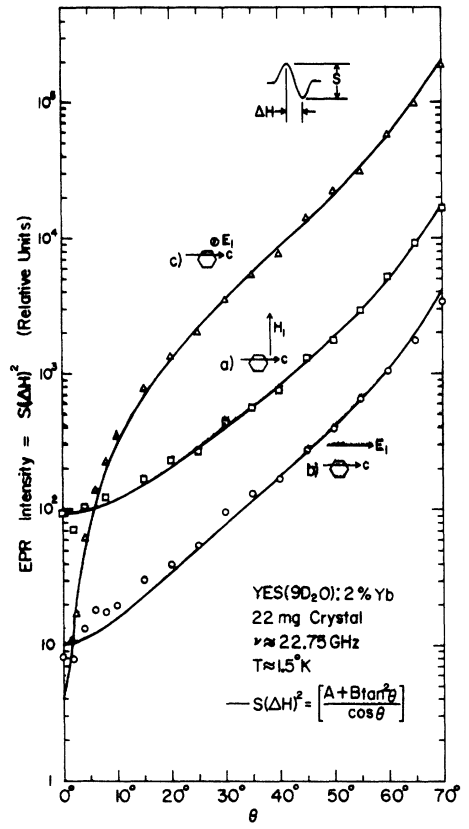

FIG. 8. Angular variation of the EPR intensity I_θ for several positions of the crystal in the cavity, as discussed in the text. The solid line is the theoretically expected form, Eq. (32), for both electric and magnetic dipole contributions.

We are actually able to estimate $g_\perp^E$ from these data, by comparing $I_{\theta=0}$ of curve a in Fig. 8 to $I_{\theta=45°}$ for curve c, using Eq. (32). We assume a constant cavity Q, undistorted cavity mode for this small sample, and $(\overline{E}_\perp/\overline{H}_\perp)^2 \approx \frac{1}{4}$ because of the dielectric constant of the sample. We have

$$\frac{I_0°}{I_{45}°} = \left(\frac{(g_\perp^0)^2 g_\parallel \cos(45°)}{g_\parallel \times \frac{1}{4} \times G^2 \tan^2(45°)}\right) \approx 10^{-2} \quad , \tag{33}$$

which, with $g_\perp^0 = 0.023$ from Eq. (21a), yields the value

$$G \cong 0.4 \quad , \tag{34}$$

to be compared to $G \geq 0.26$ from Eq. (30).

Finally, it might be useful to compare this electric dipole transition in Yb^{3+} with that observed in a non-Kramers ion. The ion Pr^{3+} in C_{3h} symmetry has approximately the following ground doublet, in terms of the basis states $|J=4, M_J\rangle$:

$$|P\rangle = \alpha|4, 4\rangle + \beta|4, -2\rangle + \epsilon|4, 1\rangle_0 ,$$

$$|Q\rangle = \alpha|4, -4\rangle - \beta|4, +2\rangle + \epsilon|4, -1\rangle_0 ,$$

where the odd-parity mixing is again due to the V_3^3 and V_5^3 crystal field terms. For this non-Kramers ion, a $\Delta M_J = 1$ electric dipole transition ($E_\perp$) is allowed directly, i.e., without the necessity of $\vec{H}\cdot\vec{J}$ admixtures from higher states, and the transition rate is orders of magnitude stronger than in Yb^{3+} and independent of θ. Culvahouse *et al.*[20] have observed such a transition for Pr^{3+} in the double nitrate crystal. The electric dipole moment in a Kramers ion is the result of the *combined* action of odd crystal field terms *and* the static Zeeman interaction.

IV. SPIN-LATTICE RELAXATION

The spin-lattice relaxation rate is calculated from first-order time-dependent perturbation theory using the relaxation perturbation[21,22]

$$\mathcal{H}_c' = \epsilon \sum_{nm} v_n^m ,$$

with v_n^m the dynamic crystal field terms and ϵ the average thermal strain due to the phonons of the lattice. The direct-process relaxation rate turns out to be

$$1/T_{1d} = w_{3/2\to -3/2} + w_{-3/2\to 3/2}$$

$$\propto \nu^3 \coth(h\nu/2kT)\left|'\langle \tfrac{3}{2}|\textstyle\sum v_n^m| -\tfrac{3}{2}\rangle'\right|^2 . \quad (35)$$

The crystal field matrix elements will vanish unless we again use the Zeeman-mixed ground states, as indicated by the primes, Eqs. (11). The lowest-order matrix elements (e.g., $\langle \frac{3}{2}|\sum v_n^m C_2| -\frac{1}{2}\rangle$) will contain the factor $H\sin\theta$, so that for $h\nu/2kT < 1$ the rate is proportional to

$$T\nu^2(H\sin\theta)^2 . \quad (36a)$$

The constant A' is then defined (using $h\nu = g_\parallel \mu_B H \times\cos\theta$) by

$$1/T_{1d} = A' H^4 \cos^2\theta \sin^2\theta\,(2kT/g_\parallel \mu_B) . \quad (36b)$$

At constant energy ($H = H_\parallel/\cos\theta$), this can be written

$$1/T_{1d} = AT\tan^2\theta . \quad (37)$$

The Raman process is proportional to T^9 and generally assumed to be angular independent. The Orbach rate is calculated by Langley and Jeffries to be negligible below 2.5 °K, in agreement with the rate $T_{10}^{-1} = 7\times10^{11}\exp(T/60\,^\circ\mathrm{K})$ measured by van den Broek and van der Marel[23] for concentrated YbES. Therefore, we have attempted to fit our data to

$$1/T_{1e} = CT^9 + AT\tan^2\theta . \quad (38)$$

A. Microwave Pulse-Recovery Data

In Fig. 9, the direct process is shown explicitly by the linear temperature dependence of T_{1e}^{-1} for a YES($9D_2O$):2% Yb crystal at $\theta = 45°$. The sample was placed in a position of maximum $E_1^\perp$ in the cavity. For this range of temperature the Raman contribution to T_{1e}^{-1} is seen to be negligible. The data fit the equation

$$1/T_{1d} = 120T\ \mathrm{sec}^{-1} , \quad (39)$$

where T is in °K. For reasons we will discuss, the recoveries were somewhat nonexponential, the initial rate being perhaps a factor of 2 faster than the tails. The data points represent the tails of the recovery, which were reasonably independent of pulse height and length.

Figure 10 shows the angular dependence at 1.53 °K of T_{1e}^{-1} for a YES($9D_2O$):2% Yb crystal located in the center of the cavity (maximum $H_1^\perp$, minimum $E_1^\perp$). The solid curve corresponds to the direct rate

$$T_{1d}^{-1} = 134T\tan^2\theta\ \mathrm{sec}^{-1} . \quad (40)$$

We wish to emphasize that the good fit of the data over two orders of magnitude to Eq. (40) for $0 < \theta < 40°$ is the first direct confirmation of the

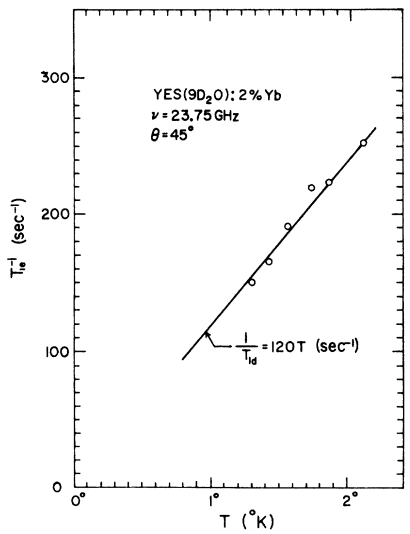

FIG. 9. Observed spin-lattice relaxation rate vs temperature displaying $T_{1e}^{-1} \propto T$, expected for the direct process.

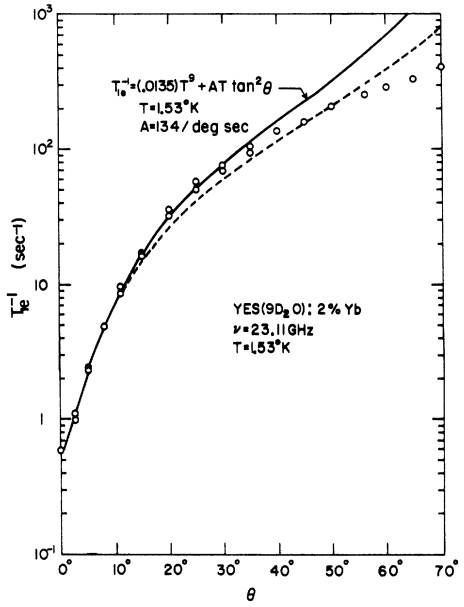

FIG. 10 Circles are observed spin-bath relaxation rate vs angle, clearly showing the expected angular dependence, Eq. (40), for the direct process for angles less than ~45°, where a phonon bottleneck begins to set in. The dotted line, Eq. (43), which includes the phonon bottleneck, fits the data better at larger angles.

theoretically expected angular anisotropy, Eq. (37), for YES:Yb. It is necessary to include the Raman rate to get a good fit. Equation (40) yields the value

$$A' = 2.4\times10^{-17}\ \text{sec}^{-1}\,\text{Oe}^{-5}\ . \qquad (41)$$

This result may be compared with $A' = 3.2\times10^{-17}$ sec^{-1} Oe^{-5} estimated by Langley and Jeffries[1] from their proton relaxation data. Langley also calculated the rate by assuming an incoherent sum

$$|'\langle\tfrac{3}{2}|\textstyle\sum v_n^m|-\tfrac{3}{2}\rangle'|^2=\sum|'\langle\tfrac{3}{2}|v_n^m|-\tfrac{3}{2}\rangle'|^2$$

and evaluating the dynamic crystal field matrix elements by the method of Orbach,[21] finding A' $= 1.4\times10^{-16}$. Ballard[3] has recently done a similar, but more refined, calculation finding $A' \approx 3\times10^{-17}$ sec^{-1} Oe^{-5}.

The deviation from $\tan^2\theta$ at higher angles is probably due to the phonon bottleneck which we estimate in Sec. IV C. Although Scott and Jeffries[22] predict an exponential recovery under some bottlenecked conditions, the rate equations are nonlinear and may lead to nonexponential recoveries.

Another likely source of nonexponential recovery is spectral diffusion in an inhomogeneously broadened line. We were able to demonstrate this by saturating the center of the YES:Yb line, i.e., "burning a hole," with no field modulation, and then watching the hole recover with field modulation, Fig. 11. We see that the spectral diffusion occurs within 1 to 2 sec, whereas the spin-lattice relaxation time $T_{1e} \approx 5$ sec. The small value of the operator $g_1^2 S_+^i S_-^j$ gives a much longer spectral diffusion time than that usually observed, e.g., by Mims *et al.*[24] for Ce^{3+} and Er^{3+} in $CaWO_4$.

B. Optical Pumping

Because of the rather long relaxation time and hence the possibility that nuclei in this crystal could be polarized by optical pumping, an experiment was conducted to determine the effect of light pumping on the electron polarization. This consisted of monitoring the EPR derivative peak and switching on and off broad-band light focused on the sample from a high-intensity mercury arc lamp. It was found that indeed there is an optical handle on the electron polarization, as shown in the insert in Fig. 12. The percent change of the electron polarization as a function of angle is also shown in Fig. 12. The effect appears to saturate for angles less than 5°. With the use of filters it was determined that this was not simply a bulk heating effect, but due to optical pumping in the 1- to 3-μ range. The exact mechanism of this optical pumping is not well understood at this time, although we tentatively ascribe it to excitation of local phonon modes around the Yb^{3+} ion. The protons are also polarized by optical pumping; this will be reported in detail later.

In this paper we will report only on the use of this optical pumping to measure the Yb^{3+} spin-

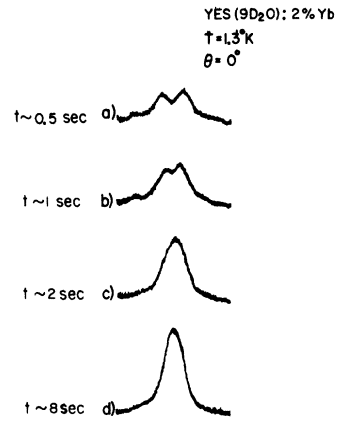

FIG. 11. EPR resonance from oscilloscope following saturation of line center without modulation field. At time $t = 0$, a 20-G peak-to-peak modulation field at 160 cps is switched on and photographs taken at successive times (a), (b), (c), and (d). This shows the recovery of a saturated "hole" in an inhomogeneously broadened line by spectral diffusion at first, followed by slower spin-lattice relaxation.

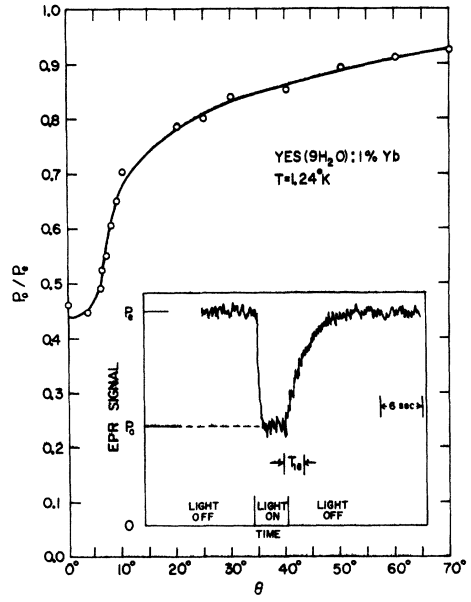

FIG. 12. Insert: optical pumping the crystal reduces the peak EPR signal from P_e to P_0; recovery occurs in a characteristic time T_{1e}. Over-all: variations of optical-pumping effect P_0/P_e as a function of angle; the solid line is a smooth line through the data points.

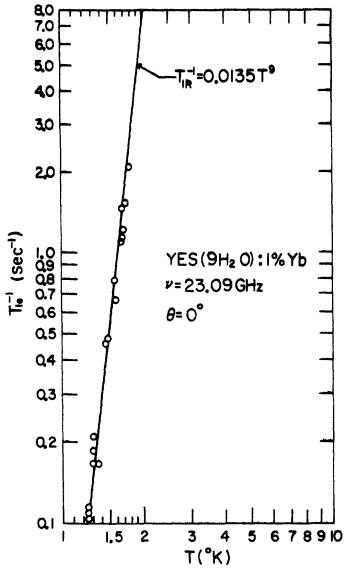

FIG. 14. Observed spin-lattice relaxation rate following optical pumping at $\theta = 0°$, where only the Raman process contributes. The solid line is Eq. (42), and clearly displays the expected T^9 dependence.

lattice relaxation time. In effect, the light takes the place of the saturating microwave pulse in the pulse-recovery experiments by changing the electron polarization from its thermal equilibrium

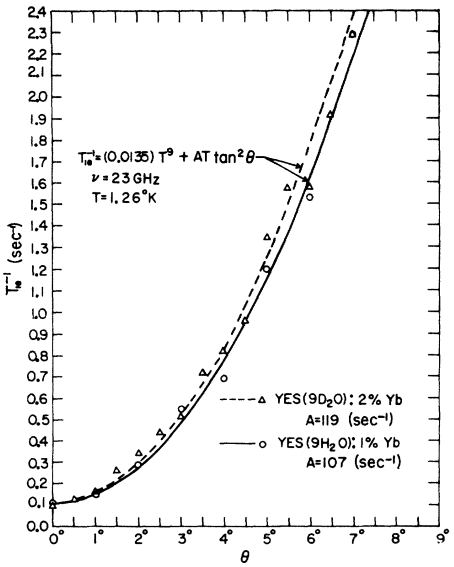

FIG. 13. Observed spin-lattice relaxation rate following optical pumping for two crystals. The lines are the best theoretical fit to a direct process plus a Raman process.

value. When the light is switched off, the polarization returns to its equilibrium value in a time T_{1e}. In this way the spin-lattice relaxation time was measured as a function of θ for small angles, Fig. 13, where it is difficult to saturate the microwave resonance. As expected, the angular dependence is explained quite well by the direct process $\tan^2\theta$. The temperature dependence at $\theta = 0°$, Fig. 14, indeed shows a pure Raman process with the rate constant

$$1/T_{1R} = 0.0135T^9 \text{ sec}^{-1} \quad . \tag{42}$$

This value is not very different from the value $T_{1R}^{-1} = 0.0155T^9$ from magnetic susceptibility measurements on concentrated YbES, [23] and the theoretical estimate $0.017T^9$ sec^{-1}. [1]

In this experiment, T_{1e} measurements were limited by the lock-in and chart recorder time constants. A glance at Fig. 12 shows that for the hydrated sample the optical saturation is effective even at $\theta = 70°$, so that direct detection of the EPR recovery with signal averaging would be a very effective way of measuring T_{1e} for all angles.

The optical pumping method has several advantages over the microwave pulse-recovery technique. Since it is a nonresonant saturation, one would expect no spectral diffusion effects—the spin recoveries should be singly exponential. This was the case for the range of temperature and angle in Figs. 13 and 14. Secondly, by the proper use of filters, there is no sample heating as in the case of high microwave powers. Thirdly, the mea-

sured recovery is independent of the recovery of the electronics following a large microwave pulse.

C. Phonon Bottleneck

Figure 10 shows that although the direct rate should increase as $AT\tan^2\theta \equiv A''T$, the observed rate above 45° is somewhat less, a behavior characteristic of the onset of a phonon bottleneck process $T_b^{-1} = DT^2$.[22] The over-all spin-bath rate is then given by

$$T_1^{-1} = \frac{A''DT^3}{DT^2 + A''T} + T_{1R}^{-1} \quad . \tag{43}$$

The bottleneck constant D for the ethyl sulfates is given by[22]

$$D \approx (l/\bar{l})g(\theta)\Delta H(\theta) \approx (l/\bar{l})200\tan\theta \quad , \tag{44}$$

where we have assumed a Yb concentration $1.2 \times 10^{19}/\mathrm{cm}^3$, a crystal thickness $l = 0.2$ cm, a phonon mean free path $\bar{l}$, sound velocity 2×10^5 cm/sec, and linewidth ΔH from Eqs. (8) and (9b). With the values $l/\bar{l} \approx 1$, $A'' = 134\tan^2\theta$, we plot Eq. (43) as the dotted line in Fig. 10. This agrees somewhat better, but not perfectly, with the data and indicates the likelihood of a bottleneck at the larger angles. In fact, an angular-dependent bottleneck constant $D \propto g(\theta)\Delta H(\theta)$ has been observed in other anisotropic crystals, LMN:Ce, LMN:Pr, and $LaCl_3$:Pr.[25]

V. SUMMARY

By considering small admixtures of excited states into the ground doublet via the static Zeeman interaction and odd-parity terms in the crystal field interaction, we have shown that the EPR transition for a Kramers ion in a crystal may be predominantly electric dipole in nature when the magnetic dipole transition rate is predicted to be weak, as it is for YES:Yb, where $g_\perp \lesssim 0.01$. By positioning a YES:Yb sample successively in the microwave magnetic and electric fields, we have found that the EPR transition is almost completely magnetic dipole when the magnetic field is along the crystal axis and predominantly electric dipole as the field is rotated away from this direction. The predicted large anisotropy of the EPR intensity due to the electric dipole contribution, Eq. (29), is in close agreement with the angular dependence of the observed intensity, which varies over five orders of magnitude; the magnitude is also in reasonable agreement with expectations. These results and the measured value of $g_\parallel$ are consistent with the usual crystal field model for the ethyl sulfate crystal, in which the symmetry of the crystal field is predominantly C_{3h}; however, small C_2 departures from this symmetry are needed to explain the intensity of the observed magnetic dipole transition at $\theta = 0°$.

Spin-lattice relaxation theory for YES:Yb predicts that the direct-process (single-phonon) relaxation is also dependent upon Zeeman mixing of excited $J = \frac{7}{2}$ states into the $J_z = \pm\frac{3}{2}$ ground doublet. Using the Zeeman-admixed ground doublet, the predicted angular dependence of the relaxation rate is $\tan^2\theta$ at constant energy and $\sin^2\theta\cos^2\theta$ at constant field. This large angular dependence has indeed been verified here, as well as the linear temperature dependence. Deviations from the $\tan^2\theta$ dependence at large angles may be partially explained by a phonon bottleneck, which is predicted to have a $\tan\theta$ dependence. A somewhat nonexponential character of signal recovery after saturation is attributed to spectral diffusion among the components of the EPR line, which is shown to be inhomogeneously broadened by a "hole burning" experiment. In addition to these microwave pulse-recovery data, an optical pumping experiment clearly showed a $\tan^2\theta$ dependence for the direct process over the range of angles observed ($\theta \leqq 7°$). Considering all of these experiments on a number of crystals, we feel the best value for the direct-process rate constant is $A' = 2.4\times10^{-17}$ $\mathrm{Oe}^{-5}\,\mathrm{sec}^{-1}$, defined by Eq. (36b). A T^9 temperature dependence of the Raman process was observed at $\theta = 0°$ using optical pumping. The Raman rate constant is measured to be $T_{1R}^{-1} = 0.01357^9$ sec^{-1}.

We measured carefully $g_\parallel$, Eqs. (21), and found that the observed 3% difference between $g_\parallel$ and $3g_L$ (for pure $J_z = \pm\frac{3}{2}$ states) could not be explained by C_{3h} or C_{3v} crystal field terms, even when J mixing is considered; thus, the virtual phonon mechanism of Inoue and Birgeneau is the probable explanation of the shifted $g_\parallel$ factor. A large angular variation in the EPR linewidth, similar to that observed in other anisotropic rare-earth crystals, is well explained by a small variation ($\Phi_{\mathrm{rms}} = 0.057°$) in the c-axis direction throughout the crystal, together with the large anisotropy in $g(\theta)$. Despite attempts to measure $g_\perp$ directly by resonance experiments, we can conclude only that $g_\perp \approx 0.01$ from line-intensity measurements.

ACKNOWLEDGMENTS

We wish to thank A. R. King and R. L. Ballard for their continued interest and many valuable discussions during the course of these experiments. We would particularly like to thank R. L. Ballard for checking some of our calculations and pointing out refinements.

APPENDIX A: J MIXING

We wish to consider mixing of the type

$$\left|\tfrac{3}{2}\right\rangle^1 = \alpha\left|\tfrac{7}{2}, \tfrac{3}{2}\right\rangle + \beta\left|\tfrac{5}{2}, \tfrac{3}{2}\right\rangle \quad ,$$

$$\left|-\tfrac{3}{2}\right\rangle^1 = \alpha\left|\tfrac{7}{2}, -\tfrac{3}{2}\right\rangle - \beta\left|\tfrac{5}{2}, -\tfrac{3}{2}\right\rangle \quad .$$

Since we are dealing with a single "hole," it is convenient to expand the $|JM_J\rangle$ states in $|M_L, M_S\rangle$ representation.

Using the appropriate Clebsch-Gordan coefficients, [26]

$$\left|\tfrac{7}{2}, \tfrac{3}{2}\right\rangle = a\left|1, +\right\rangle + b\left|2, -\right\rangle,$$

$$\left|\tfrac{5}{2}, \tfrac{3}{2}\right\rangle = -b\left|1, +\right\rangle + a\left|2, -\right\rangle,$$

$$\left|\tfrac{7}{2}, -\tfrac{3}{2}\right\rangle = b\left|1, +\right\rangle + a\left|2, -\right\rangle,$$

$$\left|\tfrac{5}{2}, -\tfrac{3}{2}\right\rangle = -a\left|1, +\right\rangle + b\left|2, -\right\rangle,$$

where $a = \sqrt{\frac{5}{7}}$ and $b = \sqrt{\frac{2}{7}}$. The perturbed energies of the ground doublet are

$$E_{|3/2\rangle^1} = {}^1\langle \tfrac{3}{2} | (-\vec{\mu}\cdot\vec{H}) | \tfrac{3}{2}\rangle^1 = (\mu_B H)^1\langle \tfrac{3}{2} | L_z + 2S_z | \tfrac{3}{2}\rangle^1$$

$$= \mu_B H[\tfrac{3}{2}g_{7/2}\alpha^2 + \tfrac{3}{2}g_{5/2}\beta^2 + 2\alpha\beta(-\tfrac{1}{7}\sqrt{10})],$$

$$E_{|-3/2\rangle^1} = \mu_B H[-\tfrac{3}{2}g_{7/2}\alpha^2 - \tfrac{3}{2}g_{5/2}\beta^2 + 2\alpha\beta(\tfrac{1}{7}\sqrt{10})],$$

where $g_{7/2} = \frac{8}{7}$ and $g_{5/2} = \frac{6}{7}$ are the Landé g factors. Therefore,

$$g_\parallel \equiv \frac{E_{|3/2\rangle^1} - E_{|-3/2\rangle^1}}{\mu_B H}$$

$$= 3.43(1-\beta^2) + 2.56\beta^2 - 1.81\beta(1-\beta^2)^{1/2}.$$

If $g_\parallel = 3.33$, then we have $\beta = +0.055$ and $\alpha = 0.9985$. Thus, to explain the observed value of $g_\parallel$ we need an admixture of about 5% $J = \frac{5}{2}$ state into the ground state. If the perturbation is $\mathcal{H}_c$, then by perturbation theory we need

$$\frac{\langle \frac{5}{2}, \frac{3}{2} | \mathcal{H}_c | \frac{7}{2}, \frac{3}{2}\rangle}{E(J=\frac{5}{2}) - E(J=\frac{7}{2})} \approx \beta \approx 0.055 \quad . \tag{A1}$$

APPENDIX B: LINEWIDTH BROADENING DUE TO "c-AXIS WANDER"

Consider a magnetic field at some angle θ_0 with respect to the "mean c axis." For this orientation of H, there will be a distribution of EPR resonant fields. A "crystallite" with a c' axis has a peak resonant field given by $H' = H_\parallel/\cos\theta'$, whereas the mean c axis represents a peak resonant field of $H_0 = H_\parallel/\cos\theta_0$. Therefore, we define $\theta' - \theta_0 = \Phi$, and $D(H' - H_0)$ = number of spins with resonance peak at H'. This is related to the angular distribution by

$$D(H' - H_0)dH' = F(\Phi)d\Phi \quad .$$

It can be shown that the measured angular deviation $\langle\Phi^2\rangle_{av}$ is small enough such that $D(H' - H_0)$ is also a Gaussian:

$$D(H' - H_0) = \frac{N}{(2\pi h)^{1/2}} \exp\left(\frac{-(H' - H_0)^2}{2h}\right) \quad ,$$

with

$$h \equiv \left(\frac{dH_0}{d\theta_0}\right)^2 \langle\Phi^2\rangle_{av} = \left(\frac{H_\parallel \sin\theta_0}{\cos^2\theta_0}\right)^2 \langle\Phi^2\rangle_{av} \quad . \tag{B1}$$

Now consider the power absorbed by a system of ions with a well-defined c' axis. This power, divided by the number of ions, can be described by the Gaussian

$$p(H - H') = p_0 \exp[-(H - H')^2/2a] \quad ,$$

where $\sqrt{a}$ represents the rms linewidth due to the local fields of the surrounding nuclei.

The total microwave power absorbed by the crystal is just the convolution of these two Gaussians:

$$P(H) = \int D(H' - H_0)p(H - H')dH'$$

$$= P_0 \exp[-(H' - H_0)^2/2b] \quad ,$$

where $b = a + h$. The observed rms linewidth is $\sqrt{b} = (a+h)^{1/2}$, and, using Eq. (B1), the derivative EPR linewidth is

$$\Delta H = 2\sqrt{b} = \left((\Delta H_n)^2 + 4\langle\Phi^2\rangle_{av} H_\parallel^2 \frac{\sin^2\theta}{\cos^4\theta}\right)^{1/2} \quad , \tag{B2}$$

where ΔH_n is the derivative "nuclear" linewidth, and θ_0 has been replaced by θ.

APPENDIX C: INTENSITY

Consider, as in Sec. III C, a paramagnetic crystal in a cavity with the c axis along the z axis, an oscillating H_1 field at frequency ν along the x axis, and a dc field H in the yz plane, with $\theta = \sphericalangle c, H$. For an EPR spectrometer it has been shown, e.g., by Feher, [27] that the spectrometer output signal voltage is $V(\nu) = KQ\eta\chi''(\nu)$, where K is an apparatus constant determined by gain, cavity coupling, detector response, and power level; Q is the cavity quality factor; η is the filling factor; and $\chi''(\nu)$ is the rf susceptibility of the sample per unit volume. The susceptibility is directly related to the power per unit volume absorbed by the sample, $P(\nu) = \pi\nu\chi''(\nu)H_1^2 = h\nu w_{rf} N_v \tanh(g\mu_B H/2kT)$, where w_{rf} is the transition probability, Eq. (17), and N_v is the number of spins per unit volume; this assumes no saturation. For a fixed position of the sample in the cavity, $N_v\eta \propto N$, the total number of spins in the sample. For constant values of Q, H, and T, we can combine these equations to obtain

$$V(\nu) \propto g_1^2 N g(\nu) \tag{C1}$$

for the resonance signal voltage, where $g(\nu)$ is the normalized line-shape function. However, it is more common to display the signal by holding ν fixed and sweeping the field H, so we introduce a normalized line-shape function $F(H)$, such that $F(H)dH = g(\nu)d\nu$. Taking $g(\nu) = F(H)(dH/d\nu) = F(H)$

$\times[h/g(\theta)\mu_B]$ in Eq. (C1) yields the resonance absorption signal as a function of field:

$$V(H) = K'[g_1^2 N/g(\theta)]F(H) \ , \qquad \text{(C2)}$$

where K' is a proportionality constant. The integrated area under the absorption signal is thus proportional to $g_1^2 N/g(\theta)$. Actually, it is customary to use a small modulation field and to observe the derivative of the absorption on a chart recorder whose deflection is

$$D \equiv \frac{dV}{dH} = K' \frac{g_1^2 N}{g(\theta)} \frac{dF}{dH} \ . \qquad \text{(C3)}$$

By assuming, say, a normalized Gaussian line-shape function $F(H) = (\sigma\sqrt{\pi})^{-1} \exp[-(H - H_0)^2/\sigma^2]$, it is straightforward to show that

$$(\Delta H)^2 S = 4K'(2/\pi e)^{1/2}[g_1^2 N/g(\theta)] \ , \qquad \text{(C4)}$$

where S is the peak-to-peak height of derivative signal D, and ΔH is the full width between inflection points of D. The quantity $(\Delta H)^2 S$ is defined as the line intensity I_θ in Eq. (19). Most previously published intensity considerations either assume isotropy or else treat $V(\nu)$ rather than $V(H)$, in which case the factor $g(\theta)$ in Eqs. (C4) and (19) drops out; it is quite important in our case. For a Lorentzian line shape $F(H) = (\delta/\pi)[\delta^2 + (H - H_0)^2]^{-1}$, Eq. (C4) becomes $(\Delta H)^2 S = (\sqrt{3}/\pi)K'[g_1^2 N/g(\theta)]$.

---

*Research supported in part by the U. S. AEC, Report No. UCB-34P20-141, 1971.

[1]K. H. Langley and C. D. Jeffries, Phys. Rev. Letters 13, 808 (1964); Phys. Rev. 152, 358 (1966).

[2] J. R. McColl and C. D. Jeffries, Phys. Rev. Letters 16, 316 (1966); Phys. Rev. B 1, 2917 (1970).

[3]R. L. Ballard, thesis (University of California, Berkeley, 1971) (unpublished).

[4]T. J. Schmugge (unpublished), quoted in Ref. 1.

[5]P. L. Scott and C. D. Jeffries, Phys. Rev. 127, 32 (1962); G. H. Larson and C. D. Jeffries, *ibid.* 141, 461 (1966); 145, 311 (1966); E. A. Harris and K. S. Yngvesson, J. Phys. C 1, 990 (1968); 1, 1011 (1968).

[6]Joel A. Dweck, thesis (Brown University, 1965) (unpublished), p. 58.

[7]A. H. Cooke, F. R. McKim, H. Meyer, and W. P. Wolf, Phil. Mag. 2, 928 (1957).

[8]R. J. Elliot and K. W. H. Stevens, Proc. Roy. Soc. (London) A218, 553 (1953).

[9]R. G. Wheeler, F. M. Reames, and E. J. Wachtel, J. Appl. Phys. 39, 915 (1968).

[10]R. J. Birgeneau, Phys. Rev. Letters 19, 160 (1967).

[11]M. Inoue, Phys. Rev. Letters 11, 196 (1963).

[12]P. L. Scott, H. J. Stapleton, and C. Wainstein, Phys. Rev. 137, A71 (1965).

[13]E. A. Gere, Bell Telephone Laboratories, Murray Hill, N. J. (private communication). We are indebted to Dr. Gere for providing us with this calibrated g-marker sample.

[14]J. H. Van Vleck, J. Phys. Chem. 41, 67 (1937).

[15]G. H. Dieke, *Spectra and Energy Levels of Rare Earth Ions in Crystals* (Interscience, New York, 1968).

[16]B. R. Judd, Phys. Rev. 128, 750 (1962).

[17]A. J. Freeman and R. E. Watson, Phys. Rev. 127, 2058 (1962).

[18]E. Y. Wong, J. Chem. Phys. 39, 2781 (1963).

[19]J. L. Prather, *Atomic Energy Levels in Crystals*, Natl. Bur. Std. (U. S.) Monograph No. 19 (U.S.GPO, Washington, D. C., 1961), Table 5.

[20]J. W. Culvahouse, David P. Schinke, and Donald L. Foster, Phys. Rev. Letters 18, 117 (1967).

[21]R. Orbach, Proc. Roy. Soc. (London) A264, 456 (1961).

[22]P. L. Scott and C. D. Jeffries, in Ref. 5.

[23]J. van den Broek and L. C. van der Marel, Physica 30, 565 (1964).

[24]W. B. Mims, K. Nassau, and J. D. McGee, Phys. Rev. 123, 2059 (1961).

[25]G. H. Larson and C. D. Jeffries, Phys. Rev. 145, 311 (1966); R. C. Mikkelson and H. J. Stapleton, *ibid.* 140, A1968 (1965).

[26]M. Rose, *Elementary Theory of Angular Momentum* (Wiley, New York, 1961), p. 224.

[27]G. Feher, Bell System Tech. J. 36, 449 (1957).

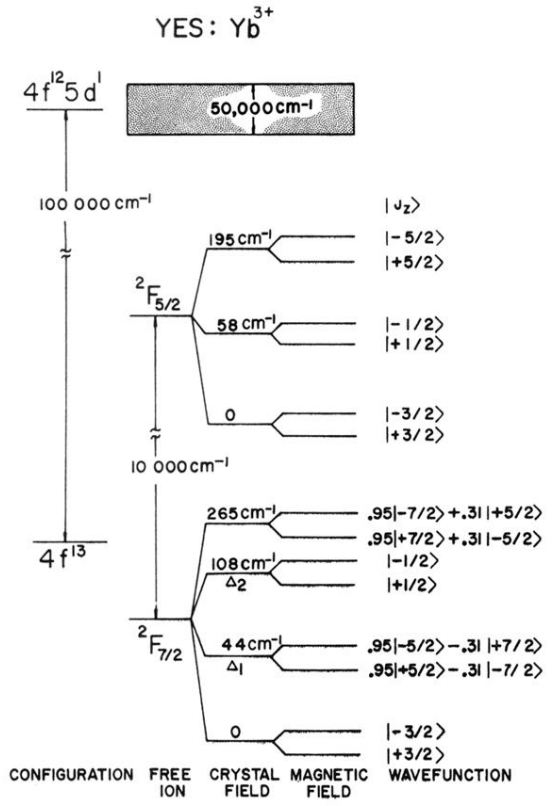

FIG. 1. Energy levels of Yb^{3+} in yttrium ethyl sulfate. For the ground multiplet $J=\frac{7}{2}$, the odd-parity wave functions for $\vec{H} \| c \| z$ are written in terms of the basis states $|J=\frac{7}{2}, J_z\rangle$. This figure is based on Ref. 1, with modifications by Ballard, Ref. 3, using new data in Ref. 9.